AIP | Review of Scientific Instruments

# Fast charged-coupled device spectrometry using zoom-wavelength optics

P. G. Carolan, N. J. Conway, C. A. Bunting, P. Leahy, R. O'Connell et al.

Citation: Rev. Sci. Instrum. **68**, 1015 (1997); doi: 10.1063/1.1147924
View online: http://dx.doi.org/10.1063/1.1147924
View Table of Contents: http://rsi.aip.org/resource/1/RSINAK/v68/i1
Published by the American Institute of Physics.

## Related Articles

Fourier transform infrared absorption spectroscopy characterization of gaseous atmospheric pressure plasmas with 2 mm spatial resolution
Rev. Sci. Instrum. 83, 103508 (2012)

Kr II laser-induced fluorescence for measuring plasma acceleration
Rev. Sci. Instrum. 83, 103111 (2012)

Laser schlieren deflectometry for temperature analysis of filamentary non-thermal atmospheric pressure plasma
Rev. Sci. Instrum. 83, 103506 (2012)

Reconstruction of polar magnetic field from single axis tomography of Faraday rotation in plasmas
Phys. Plasmas 19, 103107 (2012)

Study of the plasma wave excited by intense femtosecond laser pulses in a dielectric capillary
Phys. Plasmas 19, 093121 (2012)

## Additional information on Rev. Sci. Instrum.

Journal Homepage: http://rsi.aip.org
Journal Information: http://rsi.aip.org/about/about_the_journal
Top downloads: http://rsi.aip.org/features/most_downloaded
Information for Authors: http://rsi.aip.org/authors

ADVERTISEMENT

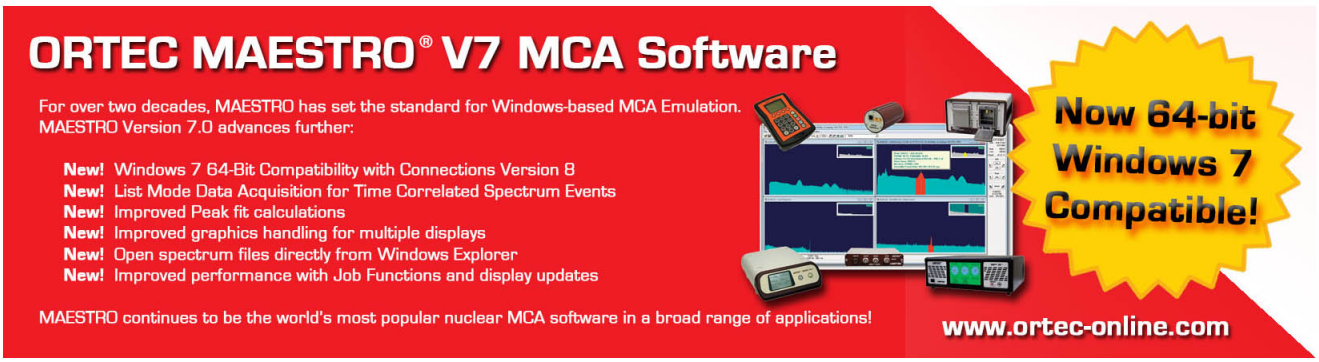

# Fast charged-coupled device spectrometry using zoom-wavelength optics

P. G. Carolan, N. J. Conway,[a] C. A. Bunting, P. Leahy,[b] R. O'Connell,[a] R. Huxford, C. R. Negus, and P. D. Wilcock
*UKAEA Fusion, UKAEA/EURATOM Association, Culham Laboratory, Abingdon, Oxon, OX14 3DB, United Kingdom*

(Presented on 16 May 1996)

Fast charge-coupled device (CCD) detector arrays placed at the output of visible spectrometers are used for multichord Doppler shift analyses on the COMPASS-D and START tokamaks. Unequal magnification in the horizontal and vertical axes allows for optimal matching of throughput and spectral resolution at the CCD detector. This involves cylindrical lenses in an anamorphic mounting. Optical acuity is preserved over a very wide range of wavelengths (220 nm→700 nm) by separate repositioning of all the optical elements which is accomplished by the use of zoom mechanisms. This facilitates rapid changes of wavelength allowing edge and core observations depending on the location of the emitting impurity ions. Changes to the ion temperature and velocity are recorded using 20 chords simultaneously with typical accuracies of $\Delta v_i < 1$ km s$^{-1}$ and $\Delta T_i/T_i < 10\%$ with a time resolution of $<1$ ms. © *1997 American Institute of Physics.* [S0034-6748(97)71501-6]

## I. INTRODUCTION

Changes to the ion pressure gradients and velocities in a tokamak plasma can occur over small extents in the spatial and temporal domains. These phenomena are often associated with the transition from low to high confinement regimes (i.e., L- to H-mode transitions),[1–4] MHD mode locking from magnetic field errors,[5–8] and magnetic island growth and rotation.[9]

Plasma impurity velocities and temperatures have been measured, using Doppler spectroscopy, on the COMPASS-D and START tokamaks with 20 chords simultaneously. These systems use 1 m grating spectrometers and fast CCD detectors that have high quantum efficiencies over a wide spectral range (e.g., 25% at 200 nm and 70% at 600 nm). The CCD row clock-down-time is short enough (0.3 and 0.6 $\mu$s) to obviate optical gating and also allows a large number of chords to be viewed without significant vertical smearing (i.e., interchord cross talk). The collected light is relayed to the spectrometers via 400 $\mu$m diameter fibers up to 20 m in length. To optimize the throughput, these are grouped in columns of four fibers for each chord and imaged onto an array of slits at the spectrometer. Photon collection efficiency is further maximized by (i) minimizing the number of lens elements and (ii) providing the different magnifications required for imaging and spectral dispersion. Cylindrical lenses are incorporated in the lens between the spectrometer and the CCD to provide this unequal magnification.

## II. DESCRIPTION OF APPARATUS

### A. CCD detector

For photon detection, we use a pair of fast two-dimensional CCD detector arrays: (i) 298×576 (horizontal ×vertical) active elements, 22.5 $\mu$m×22.5 $\mu$m, with a 0.3 $\mu$s row shift time, and (ii) 385×288 active elements, 22 $\mu$m×22 $\mu$m, with a 0.6 $\mu$s row shift time, which are about an order of magnitude faster than typical cameras. The CCD sensors have fluorescent coatings which extend the UV sensitivity to about 200 nm and are Peltier cooled to reduce the dark current and to increase the effective dynamic range. Several rows are illuminated for each spectrum. These are vertically compressed, or binned, into single rows and stored in masked region of the chip while, a discharge is in progress. This allows for fast spectrum recording ($\lesssim$1 ms) and is very convenient for plasmas of relatively short duration (i.e., $\lesssim$1 s). Since each row in the storage area records spectra from five slits, in the present arrangement, between ~1400 and ~2800 spectra, depending on which camera is used, can be recorded in this way. Optical gating is not required because the fast CCD row charge transfer time allows the detected charges to be swept through the illuminated CCD elements fast enough so that the extra signal gathered is insignificant. This is a considerable advantage as mechanical optical gates are too slow and using a photocathode-based image intensifier carries a severe penalty with its order of magnitude lower quantum efficiency. The binned CCD element charges are amplified and digitized only after the discharge is over and stored locally in the data acquisition PC and then transferred to a mainframe for later analyses. The PC is also used for spectrometer alignment and calibrations even while an experimental program is in progress.

### B. Optics and spectrometer

#### *1. Collection optics and fibers*

A modular collection lens was designed using off-the-shelf lens elements, all from UV grade quartz. Conventional achromatic optics are inappropriate because of the short wavelengths and the further demands of large aperture and the wide spectral range required. Since the spectral bandwidths from the Doppler shifts are relatively narrow, simple lenses of a single material can be used. Changes in the central wavelength are accommodated by repositioning the lens elements. This mechanical requirement is similar to that used in conventional variable focal length camera lenses. Such a zoom lens mechanism, as illustrated in Fig. 1, provides the

[a]Present address: University College Dublin, Republic of Ireland.
[b]Present address: University College Cork, Republic of Ireland.

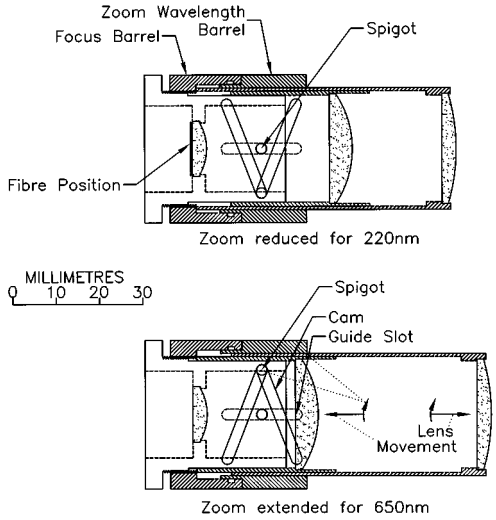


FIG. 1. Collection lens with short and long wavelength settings. When the zoom-wavelength barrel is rotated it moves the lenses by distances determined by the pitch of the cams on the lens tubes.

necessary lens movements while retaining the other optical properties (viz. telecentricity, flat image plane, constant chord view angles and magnification). (This zoom adaptation is also used for the input lens to the spectrometer and the output coupling lens to the CCD detector array.) The collection lens is composed of three elements, cf. Fig. 1, and provides 15° field-of-view and a flat image plane for object distances from 0.5 m→1.5 m.

The $f/2$ output and telecentric imaging are ideal for the coupling to the fiber bundles. These are arranged in groups of four 400 $\mu$m diameter quartz fibers which are separately mounted in metal holders at the collection optics and spectrometer, giving up to ten viewing chords. The angle of each of the lines-of-sight illuminating the fiber bundles is maintained as the zoom mechanism is adjusted for the design range of wavelengths (220 nm→700 nm).

Examples of the measured relative responses of the fiber bundles are shown for one of the collection lenses in Fig. 2 for a particular wavelength (636 nm). The very modest falloff in response at the edges is due to slight vignetting. The compactness of the collection lens design (30 mm in diameter) allows the complete lens assembly to be used for the various views available on COMPASS-D and START. By keeping the fiber lengths as short as possible we can access shorter wavelengths, viz. 7 m on START allows observation of heliumlike carbonfive (227 nm) and $B^{3+}$ (282 nm) while the 20 m on COMPASS-D gives a correspondingly longer wavelength cutoff where only the heliumlike boron can be used.

### 2. Spectrometer

Visible spectrometers (Hilger Analytical; $f/10$, 1 m focal length, Czerny–Turner mount) are used to disperse the spectra using a variety of gratings (e.g., 2400 g/mm holographic, 2160 g/mm blazed for 500 nm and *echelle* gratings with 79 g/mm[6] and 316 g/mm[10]). To date the greatest number of chords is from the START experiment, to exploit the diagnostic features associated with the neutral beam (NB) (i.e.,

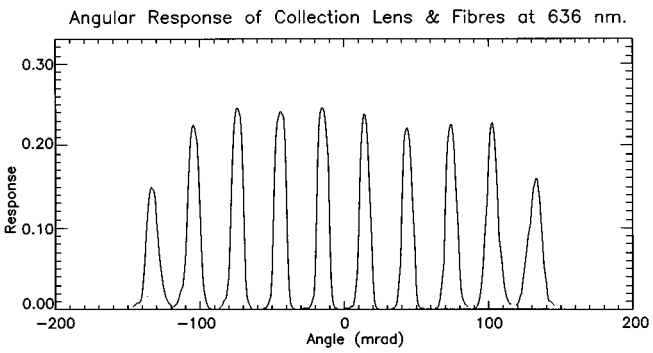


FIG. 2. Relative response curves of the ten fiber bundles, 4×400 $\mu$m diameter, from one of the $f/2$ 15° field-of-view collection lenses.

charge exchange recombination spectroscopy (CXRS) and beam emission spectroscopy (BES). Light from 20 views of the START plasma illuminates a 4×5 array of slits (typically 400 $\mu$m wide), laser cut into a metal foil, at the input of the spectrometer preceded by image and aperture optimizing optics. The foil is mounted on a movable alignment carriage.

The grating ruling density is chosen to fulfil satisfactorily the conflicting requirements. First of all it is desirable to observe the maximum number of detected spectra without spectral overlap, or interchord cross-talk. This requires a low dispersion grating. On the other hand optimizing the *etendu*, or time resolution, and the spectral, or velocity, resolution, requires high dispersion. Another complicating factor is the large spectral range required which limits the ruling density and necessitates either a flat spectral response, say from a holographic grating, or to use a blazed grating in different orders.

The criteria chosen were for up to 20 detected lines-of-sight and typical accuracies of 10%→20% in ion temperature and 1 km $s^{-1}$ in ion velocities both with ~1 ms time resolution. The photon fluxes were based on measured line intensities from resident impurities, primarily emitting at the outer regions, and central ion temperatures and line intensities expected from charge exchange transitions using a 10 Å 40 kV neutral beam at typical densities in START and a 1 Å 60 kV diagnostic neutral beam in COMPASS-D. The spectral response functions, corresponding to each of the slits, are measured with the completely installed system, from the collection lens to the CCD. Narrow emission lines from a spectral lamp (e.g., nickel, mercury) are used to illuminate the collection lens with a wavelength close to the plasma line of interest. Instrument functions from all the slits are obtained, which automatically caters for spectrometer focusing effects and aberrations, for slit profiles including the detailed imaging of the fibers at the slits. These instrument functions are used in unfolding the data in terms of ion temperature and velocity and the line intensities from convolved best fits to the recorded spectra.

### 3. Input and output spectrometer optics

The input optics and output optics were designed as part of a complete system, including the spectrometer and the CCD detector array, to optimize the optical acuity, light col-

lection power and matching of image magnification on the CCD to satisfy the demands of multichord observation and the spectral separation and resolution requirements. From the measured angular dependence of the fiber output light brightness, a modest factor of 2 magnification of fibers (400 $\mu$m diameter) to the input slits (typically, 400 $\mu$m wide) is sufficient for efficient light gathering by the spectrometer ($\sim f/10$), even though only $f/5$ aperture of the fiber emission is used. This magnification also allows several rows of fiber bundles to be imaged through the spectrometer to the CCD. The lens elements of both the input and output optics lenses were custom designed and use the minimum number of elements to minimize reflection losses. This is important as the wavelength range required precludes the use of antireflection coatings.

To image the spectra onto the CCD sensor, an anamorphic lens system is used to change the aspect ratio of the image by $\sim$1.5, i.e., a demagnification of 3 in height and 2 in length (i.e., in the spectrum dispersion direction). (The system was also slightly astigmatic to correct the astigmatism of the spectrometer and so reduce the up–down cross-talk of the spectral rows.) The unequal demagnification also, effectively, increases the *etendu* of the system, while maintaining high spectral resolution. We choose that the image width of each slit ($\sim$200 $\mu$m) should be of the same order as the typical Doppler width rather than the convention of being much smaller. This is to increase the photon statistics and results in generally superior accuracy in determining the spectral width and position and is particularly efficacious when the spectral instrument functions have sharp leading and falling edges as indicated by Monte Carlo simulations of the photon statistics. The same philosophy, as used in the collection lens, of using one material lens elements and relying on zoom-wavelength mechanisms is also used for both optical systems, one of which is illustrated in Fig. 3. The use of these zoom-wavelength systems throughout allows rapid changes of the operating wavelengths providing maximal use of the spectrometers. However, greater care has to be exercised in the positioning of the spectrometer lens elements. Changes to the optical acuity, especially in the coupling optics from the spectrometer to CCD, alter the spectral instrument functions, particularly affecting the unfolding of spectral widths. For example, an error of $\pm 0.25$ mm in the zoom barrel position (50 mm diameter) would be reflected in temperature errors of $\sim$35 eV at 300 nm and $\sim$10 eV at 600 nm for an oxygen impurity line. These errors are for the image positions suffering the greatest defocusing.

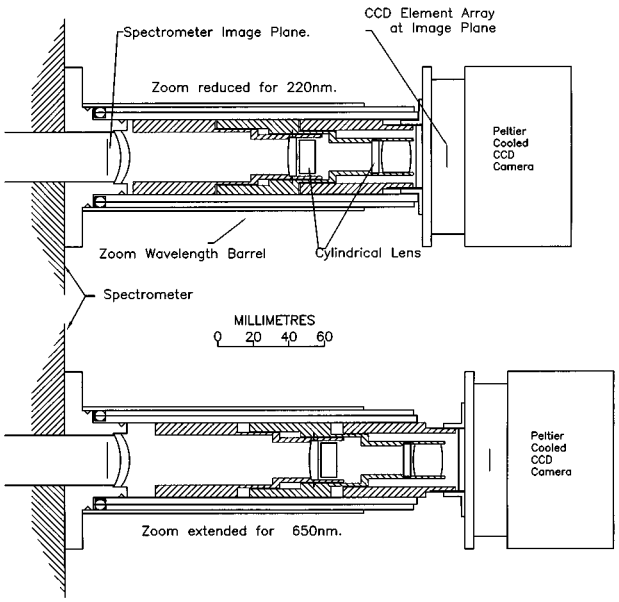


FIG. 3. Anamorphic lens that couples the dispersed spectra to the CCD detector array. Cylindrical lens elements are used to achieve the unequal vertical and horizontal (spectral) magnification. A zoom-wavelength system is also incorporated.

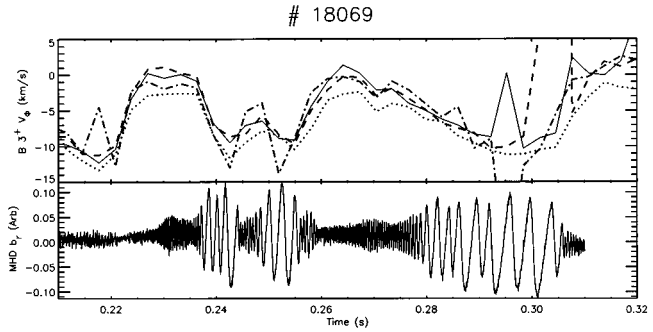


FIG. 4. Comparison of Doppler $B^{3+}$ (282 nm) $V_\phi$ velocities from four chords on COMPASS-D and the MHD radial magnetic field, $b_r$, waveform in the presence of a magnetic island.

## III. EXPERIMENTAL RESULTS

To illustrate the use of the versatility of the instrument design both in terms of wavelengths and observable plasma phenomena, we show results from the COMPASS-D and START devices in the presence of magnetic islands and the injection of a heating neutral beam, respectively.

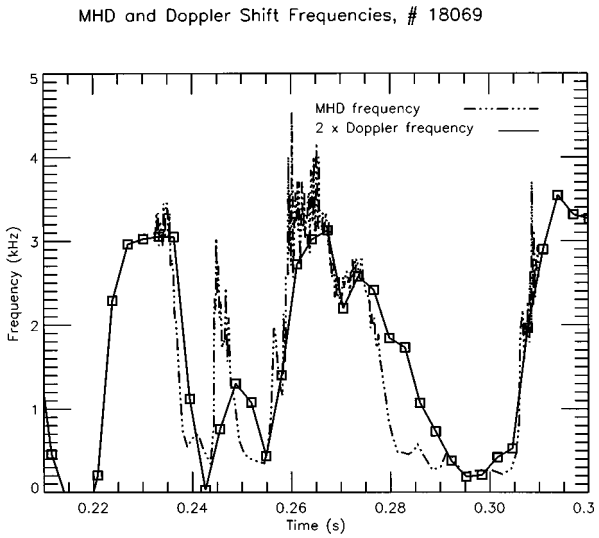


FIG. 5. The data from one of the chords and the $b_r$ waveform in Fig. 4 are here compared in terms of toroidal frequency.

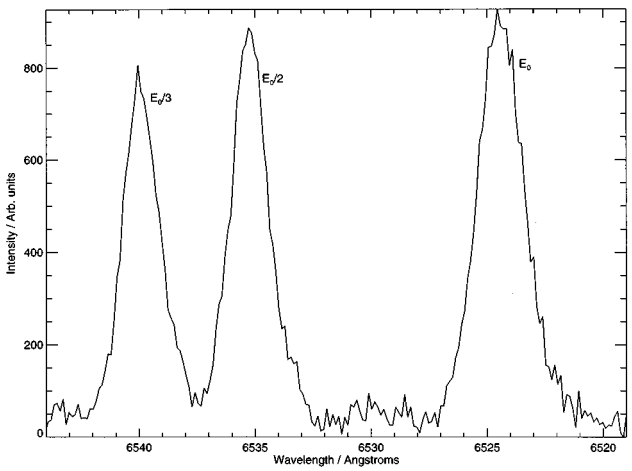


FIG. 6. Doppler shifted $H_\alpha$ spectrum arising from the $E_0$, $E_0/2$, and $E_0/3$ energy components measured from the neutral beam atoms on the START device.

A fan of views in the equatorial plane of COMPASS-D is used to monitor the toroidal ion velocities and temperatures, in this case of the $B^{3+}$ ions which radiate a few cm in from the periphery. In Fig. 4 the toroidal rotation from four of the chords is compared with the radial magnetic field perturbation associated with the growth of a magnetic island and its changes in velocity.[9] (The error bars on these data have been estimated using a Monte Carlo simulation method for generating sample spectra, which are then fitted in the normal way. From the fits, the scatter on the fitted velocity may be calculated. Here the typical velocity error bar ($2\times\sigma$) is $\pm 0.9$ km $s^{-1}$.) The correlation between the toroidal velocity and MHD effects can be seen more readily when both are expressed in terms of toroidal frequency as shown in Fig. 5 using just one of the lines-of-sight. Apart from a factor of $\sim 2$ difference between the two frequencies, previously observed in similar locked MHD mode experiments,[7,8] the two track each other quite well with a slightly longer decay time from the ions, probably due to a combination of viscous forces[5] and frictional effects between impurity ions and the other particles.

A 30° fan of 20 viewing chords in the equatorial plane of the START device similarly monitors temperature and velocity distributions of a spectrally selected impurity ionization state. The spectrometer can also be used to monitor the neutral beam energy components from relatively long wavelengths, $H_\alpha$ (656 nm), and an example is shown in Fig. 6 exhibiting three spectral peaks from the separate energy components in the beam. These results are used to optimize the beam characteristics.

## ACKNOWLEDGMENTS

This work is funded by the UK Department of Trade and Industry and EURATOM.

[1] P. Gohil *et al.*, in Proceedings of the 18th EPS Conference on Controlled Fusion and Plasma Physics, Berlin, 1991 (unpublished), Vol. 15C, Part I, p. 289 (1991).
[2] A. R. Field *et al.*, Nucl. Fusion **32**, 1191 (1986).
[3] P. G. Carolan *et al.*, Plasma Phys. Control. Fusion **38**, Suppl(7) A, A111, (1994).
[4] P. G. Carolan, R. O'Connell, and N. J. Conway, Bull. Am. Phys. Soc. **40**, 1762 (1995).
[5] T. C. Hender *et al.*, Nucl. Fusion **32**, 2091 (1992).
[6] R. A. Bamford, P. G. Carolan, and C. A. Bunting, Rev. Sci. Instrum. **63**, 4962 (1992).
[7] A. W. Morris, P. G. Carolan, R. Fitzpatrick, T. C. Hender, and T. N. Todd, Phys. Fluids B **4**, 413 (1992).
[8] P. G. Carolan, R. Fitzpatrick, T. C. Hender, and A. W. Morris, in Proceedings of the 19th EPS Conference on Plasma Physics, Innsbruck, 1992 (unpublished), Vol. 16C, Part I, p. 411 (1992).
[9] D. A. Gates and T. C. Hender, Nucl. Fusion **36**, 273 (1996).
[10] P. G. Carolan and R. O'Connell, Rev. Sci. Instrum. **66**, 1184 (1995).